THE JOURNAL OF PHYSICAL CHEMISTRY C
A JOURNAL OF THE AMERICAN CHEMICAL SOCIETY

pubs.acs.org/JPCC
Article

Niobium Oxide Films with Variable Stoichiometry: Structure, Morphology, and Ultrafast Dynamics

Published as part of The Journal of Physical Chemistry C special issue "Francesc Illas and Gianfranco Pacchioni Festschrift".

Samuele Pelatti, Stefania Benedetti, Giuseppe Ammirati, Patrick O'Keeffe, Daniele Catone, Stefano Turchini, Xinchao Huang, Yohei Uemura, Frederico Lima, Christopher Jackson Milne, and Paola Luches*

Cite This: J. Phys. Chem. C 2025, 129, 8206−8214

ABSTRACT: Niobium oxide can be stabilized in three distinct stoichiometries, each exhibiting unique physicochemical properties relevant to various technological applications. This study presents a novel procedure for fabricating niobium oxide films and tuning their stoichiometry among the three most stable oxide phases. Starting with a magnetron-sputtered film predominantly composed of Nb_2O_5, its structure and stoichiometry are optimized through thermal treatment in an O_2/N_2 flux. A vacuum reduction treatment transforms the as-grown film into the NbO phase, which can then be reoxidized under controlled oxygen partial pressure to achieve the NbO_2 phase. The films are characterized in terms of surface composition using X-ray photoemission spectroscopy, structure through X-ray diffraction, optical properties via UV−vis spectrophotometry, and morphology using scanning electron microscopy. Additionally, we show that X-ray absorption near-edge spectroscopy at the Nb K-edge, performed with X-ray free-electron laser radiation, can provide insights into the electronic structure and subsurface stoichiometry of the films. The ultrafast mechanisms underlying photoinduced processes in NbO_2 are also discussed.

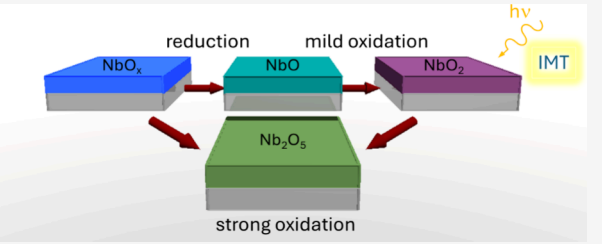

INTRODUCTION

Niobium oxide films exhibit interesting optical and electrical properties, making them relevant for various technological applications such as solid electrolytic capacitors, transparent conductive oxides, photochromic devices, memristors, dye-sensitized solar cells, and more.[1−3] Niobium oxides exhibit three relatively stable stoichiometries: NbO, NbO_2, and Nb_2O_5, each characterized by distinct physicochemical properties. Among these, Nb_2O_5, containing Nb ions in the 5+ oxidation state, is the most thermodynamically stable phase. It exists in different crystalline polymorphs[4] and is used as a photocatalyst due to its strong redox ability,[3,5,6] as well as in Li-ion batteries.[2] The NbO phase, in which the cations adopt the lowest +2 oxidation state, has an ordered cubic structure in the $Pm\bar{3}m$ space group. NbO is a conducting oxide with a superconductor behavior at 1.38 K.[7] It is used in capacitors in combination with Nb_2O_5 as a dielectric.[7,8] A further thermodynamically stable phase is NbO_2, in which the cations adopt the intermediate 4+ oxidation state. NbO_2 shares similarities with other strongly correlated oxides, such as VO_2, with both materials exhibiting a thermally induced insulator-to-metal transition (IMT) at a material-dependent critical temperature of 70 °C for VO_2 and 810 °C for NbO_2. In VO_2, the IMT is said to take place via a cooperative interplay between the Mott (electron−electron correlation) and Peierls (electron−lattice coupling) mechanisms,[9] although distinguishing between these two mechanisms in the case of photoinduced IMT is difficult due to the low critical temperature in this material. On the other hand, the thermally induced IMT in NbO_2 occurs at a much higher temperature (1080 K) and involves a transition from a body-centered tetragonal semiconducting phase to a rutile metallic phase. The Nb 4d electrons in NbO_2 are less localized and energetically more dispersed compared to VO_2, resulting in weaker electron correlation. However, the Nb−Nb dimerization suggests the possibility of Peierls-driven insulating behavior. The literature remains divided on the precise nature of the phase transition in NbO_2. Theoretical studies propose that NbO_2 exhibits Peierls-like mechanism,[10] while other works emphasize a Mott-dominated transition.[11,12] The abrupt change in conductivity

Received: December 17, 2024
Revised: February 27, 2025
Accepted: March 11, 2025
Published: April 18, 2025

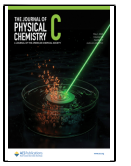

https://doi.org/10.1021/acs.jpcc.4c08535
J. Phys. Chem. C 2025, 129, 8206−8214

has interesting applications in memresistive devices, ultrafast electrical switches and thermal sensors.[13]

Nb_2O_5 and NbO_2 are known to be indirect band gap semiconductors.[14] The indirect gap observed in the literature for reference Nb_2O_5 samples ranges from 3.0 eV on commercial powders,[15] to 3.4 eV on films prepared by dual ion assisted deposition[16] and 3.3−3.5 eV in films directly obtained by magnetron sputtering in high oxygen flux.[17] The value of the indirect bad gap for NbO_2 is approximately 0.7−1.2 eV.[18]

As for various other transition metal oxides, an interesting topic is the possibility to modify the properties by light irradiation. Interesting research lines in this field are for example studies of photoexcitations in materials including Nb_2O_5, relevant for a detailed description and optimization of photocatalytic activity.[19,20] In NbO_2, in analogy with the case of vanadium dioxide,[21−23] it was shown that the thermally induced phase transition can also be triggered by light absorption,[11,23] a very appealing aspect in view for example of application in ultrafast switches. However, in the case of NbO_2 the detailed atomic scale mechanisms that drive the transition are still largely unknown. In particular, the role of electronic correlations and the interaction with the lattice in the transition are still largely debated.[11,12,23−25] A detailed understanding of the transition mechanism, besides being interesting for basic science, may lead to a design-driven optimization of the material for application in devices.

Previous works have focused on the growth of niobium oxide films in a specific stoichiometry. In particular, physical synthesis methods have been used to grow films with thickness from several tens to several hundreds of nm using pulsed laser deposition[14,26] or magnetron sputtering,[17,27,28] either using pressed oxide powder targets[27] or metallic Nb targets in controlled conditions of temperature and O_2/Ar flux.[17,28,29] However, achieving a high degree of control of the stoichiometry in niobium oxide films during the growth and being able to achieve the different stoichiometric phases resulted to be a quite challenging task. Using reactive deposition in different conditions of temperatures and O_2/Ar flux many earlier studies reported only the formation of a dominant Nb_2O_5 phase with minor changes in the degree of crystallinity and in the optical and electric properties.[30−32] Moreover, the high reactivity of Nb to O_2 severely affects the deposition rate[17] and additionally complicates the stoichiometry control. More recently, Hossein and co-workers managed to obtain the NbO_2 and the Nb_2O_5 phase using different growth temperatures and O_2/Ar ratio.[17] The use of postgrowth treatments is highly desirable to allow for a obtaining the different oxide phases without the need of optimizing the growth parameters, often dependent on the specific apparatus used. This approach was used by Logacheva et al., who used post growth treatments in O_2 at different temperatures to obtain NbO_2 and Nb_2O_5, but the study is limited to the analysis of the structure and surface morphology of the films.[33]

This work aims to describe a robust procedure for obtaining niobium oxide films in the three stable stoichiometries through thermal treatments under oxidizing and reducing conditions. Briefly, the procedure starts from a film in the most stable Nb_2O_5-like stoichiometry that is then reduced in vacuum to obtain a dominant NbO phase and can be later reoxidized in controlled O_2 partial pressure to obtain a dominant NbO_2 stoichiometry. The Nb_2O_5 stoichiometry can be reobtained by heating in O_2 flux. The advantage of the procedure described here is that it allows us to obtain niobium oxide films in the three different stoichiometric phases starting from a single film. A complete characterization of the three different oxides in terms of structure, optical properties, morphology and surface composition is reported. Furthermore, the NbO_2 films are also characterized by Femtosecond Transient Absorption Spectroscopy (FTAS), to investigate the photoinduced IMT, exploring how the ultrafast dynamics are affected by excitation energy and intensity, and discussing the observed ultrafast transient absorbance with reference to recent works.

The results obtained provide a reference for perspective studies of the dynamics of light-induced processes using element-sensitive ultrafast X-ray techniques. As a first step in that direction, we show and discuss also X-ray absorption near-edge spectroscopy (XANES) measurements at the Nb K edge acquired on some of the films using ultrashort high-energy photon pulses generated by the European X-ray Free Electron Laser (EuXFEL). The feasibility of such high-energy measurements, that provide accurate information on the electronic properties of the films, pave the way for future studies of light-induced processes in the investigated materials.

EXPERIMENTAL PROCEDURES

The substrates used for the growth of niobium oxide films were (100) Si wafers with a 600 nm surface thermal oxide film for X-ray photoemission spectroscopy (XPS) and X-ray diffraction (XRD) measurements. UV-grade fused silica substrates were instead used for UV−vis spectrophotometry measurements that require transparent supports. Both kind of substrates were cleaned with a bath in acetone at 150 °C for 5 min, followed by an ultrasonic bath in acetone and an ultrasonic bath in isopropanol at 80 °C for 3 min.

The niobium oxide films were grown by reactive magnetron sputtering, using a 3 in. metallic Nb target and a DC current at a power of 125 W in a flux of 1 sccm of O_2 and 20 sccm of Ar. The substrate was heated at a temperature of 500 °C during the deposition.

The thickness of the films was controlled during the growth by a quartz microbalance, calibrated by a stylus profilometer. The films investigated here have a thickness of 150 nm. The uniformity of the thickness after growth was checked by stylus profilometry in different positions along a line across the surface.

The optimized procedures to obtain the different dominant stoichiometries are schematically shown in Figure 1. After deposition, to obtain a pure Nb_2O_5 film, the sample was annealed using a tube furnace at 600 °C in 50% O_2 and 50% N_2 flux at 5 bar for 1 h. To obtain NbO, the deposited NbOx film was annealed in ultrahigh vacuum (UHV) at $P = 1 \times 10^{-9}$ mbar at 600 °C for 1 h. After reduction, to obtain NbO_2, the NbO samples were further annealed at 750 °C in vacuum at $P = 1 \times 10^{-6}$ mbar of oxygen for 1 h.

XPS was used to determine the stoichiometry of the samples after the growth and during the treatments by measuring the evolution of the Nb 3d line shape. The XPS measurements were performed in a UHV apparatus equipped with a double-anode Mg/Al K_α X-ray source and a hemispherical electron analyzer. For the present experiments Al K_α photons were used and the XPS spectra were collected at normal emission geometry. Quantitative information on the sample stoichiometry were obtained by fitting the Nb 3d spectra using three Voigt shaped doublets with width, branching ratio and binding energy as reported in the Supporting Information (Table S1).

https://doi.org/10.1021/acs.jpcc.4c08535
J. Phys. Chem. C 2025, 129, 8206−8214

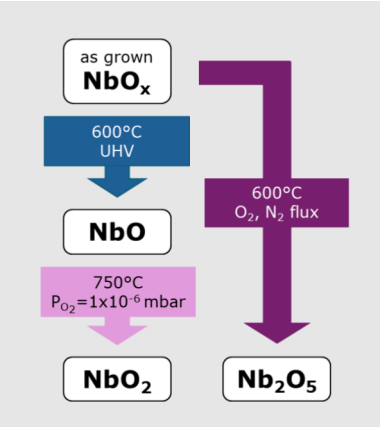

Figure 1. Flowchart describing the procedures to obtain the three different niobium oxide stoichiometries.

These values are consistent with previously published results found in refs 34, 35.

UV−vis spectrophotometry was used to assess the optical absorptance of the samples. The apparatus used was equipped with a Xenon light source to produce a white light emission spectrum and the desired wavelength was selected and scanned by using a grating monochromator. In this study, the optical properties of the samples were studied in a wavelength range from 250 to 800 nm. A linear polarizer after the monochromator was used to select light with s polarization. A silicon photodetector was used to measure the intensity of the light transmitted or reflected by the sample. In the geometry used during the experiment, the sample normal formed an angle of 22° with the incident light. The transmittance T and reflectance R were measured and the absorptance A was obtained as $A = 1 - (T + R)$.

X-ray diffraction (XRD) was used to characterize the crystallinity of the films and the different structural phases present. The XRD measurements were acquired using a Bragg−Brentano 2θ-ω apparatus with Cu K_α photons. The diffraction circle had a radius of 240 mm, and a proportional point detector was used.

A Scanning Electron microscope (SEM) with a field emission gun was used to image the surface morphology of the samples.

The FTAS measurements were conducted using a femtosecond laser system that produces 35 fs pulses at 1 kHz with a pulse energy of 4 mJ. The pump pulses at 535 nm wavelength were generated using the output of an optical parametric amplifier, covering the tunable energy range of the pump pulse. The probe beam was a white light supercontinuum spanning 250−1600 nm, generated in a commercial TA spectrometer (FemtoFrame II, IB Photonics) using different setups depending on the spectral range.[36] In the TA experiments, the pump and probe beams were focused on the sample with diameters of 200 and 150 μm, respectively. The temporal delay between the pump and probe was varied by adjusting the optical path length of the probe. Successive acquisitions on the same sample spot indicated that the material was not permanently changed within the fluence range investigated (up to 33 mJ/cm^2).

The XANES measurements were acquired at the FXE instrument of the European XFEL facility.[37,38] The XFEL pulse was delivered in train mode, using 20 pulses per train at a repetition rate of 282 kHz and 10 trains per second, i.e., 200 pulses per second. The X-ray pulse duration was 50 fs fwhm. The pulse energy from the undulator source was ∼450 μJ. A two-bounce Si(111) monochromator provided a monochromatic beam with energy resolution $\Delta E/E \sim 10^{-4}$ and the incoming beam flux was estimated to be ∼10^9 photons/pulse. The photon energy was scanned across the near range of the Nb K-edge (18,970−19,040 eV). The beam was focused by compound refractive lens to a spot size with a diameter of approximately 20 μm. The incoming beam intensity was measured by monitoring the scattering signal from a thin Kapton film. The XANES measurements were performed at room temperature in total fluorescence yield. Biased PIN diodes and digitizer (2 Gs/s, 12 bits) were employed as the detection system, and a Zr filter with μT ∼ 3 was installed in front of the fluorescence diode sensor. The correlation between the incoming pulse intensity and fluorescence signal was checked before the XANES measurement. Due to the stochastic nature of XFEL pulses that originate from self-amplified stimulated emission (SASE) mode, the monochromatic beam intensity fluctuates from pulse to pulse, so low and high thresholds were applied to filter out the weakest and strongest pulses from the digitizer raw data.

RESULTS AND DISCUSSION

The changes in stoichiometry induced in the niobium oxide films by the various thermal treatments can be identified by the modifications in shape of the Nb 3d XPS spectra, shown in Figure 2. After growth, the films have a dominant Nb_2O_5 stoichiometry (see Supporting Information, Figure S1). To optimize the Nb_2O_5 stoichiometry the film was heated at 600 °C in O_2 and N_2 flux in ambient pressure for 1 h. The Nb 3d XPS spectrum (Figure 2a) shows the presence of two well-

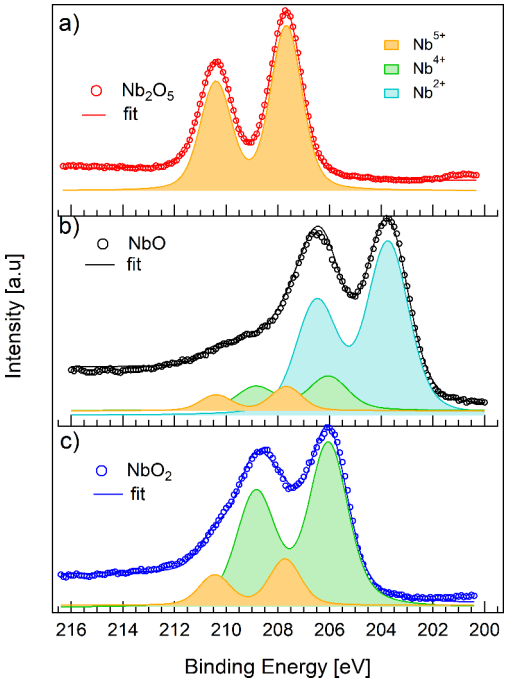

Figure 2. Nb 3d XPS spectra of the niobium oxide film, after the thermal treatments detailed in Figure 1, and corresponding fit (solid lines). The individual Nb^{5+}, Nb^{4+}, and Nb^{2+} components used for the fitting are also shown.

https://doi.org/10.1021/acs.jpcc.4c08535
J. Phys. Chem. C 2025, 129, 8206−8214

defined peaks at 210.1 and 207.4 eV, which are characteristic of the Nb_2O_5 phase.[26]

When the as-grown sample is annealed in UHV at 600 °C for 1 h the Nb 3d XPS spectrum (Figure 2b) shows a significant change of shape with two dominant peaks appearing at lower binding energies, 206.5 and 203.7 eV, characteristic of the NbO phase.[39] A further annealing of the NbO film at 750 °C in an O_2 pressure of $P = 1 \times 10^{-6}$ mbar for 1 h results in a further change of spectral shape (Figure 2c) with the two main peaks shifting to 208.2 and 205.6 eV, characteristic of the NbO_2 phase.[17] When comparing the XPS spectra of the different niobium oxide phases to the peaks of the Nb_2O_5 phase, the peaks of the NbO and NbO_2 films appear qualitatively broader, they apparently deviate from 2:3 branching ratio and they show a certain degree of asymmetry toward higher binding energies with respect to those of the Nb_2O5 phase. This evidence suggests the presence of minority phases, in addition to the dominant one. The fits of the spectra, using three doublets related to Nb^{5+}, Nb^{4+}, and Nb^{2+}, reported in Figure 2 (see also Supporting Information, Table S1), show that the Nb_2O_5 film has a 100% Nb^{5+} oxidation state, while the NbO film has a 77% Nb^{2+}, 15% Nb^{4+}, and 8% Nb^{5+} concentration, with the minority phases possibly deriving from partial surface oxidation as confirmed by XPS spectra acquired at grazing emission (see Supporting Information, Figure S2). The NbO_2 film is composed of 82% Nb^{4+} and 18% Nb^{5+}, where the Nb^{5+} ions are located preferentially at the surface also in this case. It has to be noted that XPS is a very surface-sensitive technique with a probing depth of only a few nm at normal emission. Therefore, the measured concentration of nonstoichiometric phases measured by XPS for the NbO and NbO_2 samples may possibly be limited to the film surface, as suggested by the spectra acquired at grazing emission (see Supporting Information, Figure S3).

XRD measurements were performed in order to assess the degree of crystallinity of the films. Figure 3 reports 2θ-ω scans for the three different films. The diffraction pattern of the Nb_2O_5 film (red line in Figure 3) contains several peaks with a very small intensity that can be attributed to the simultaneous presence of different crystallographic phases: a monoclinic, an orthorhombic and a tetragonal phase, in agreement with the literature.[17] The XRD pattern of the NbO film (black line in Figure 3) contains significantly more intense peaks, as compared to the Nb_2O_5 phase, possibly deriving from a higher degree of crystallinity. The most intense peak at 42.5° can be ascribed to NbO(200), the intermediate intensity peak at 36.7° to NbO(111) and the low intensity peak at 61.8° to NbO (220) (JCPDS 01-078-0723).

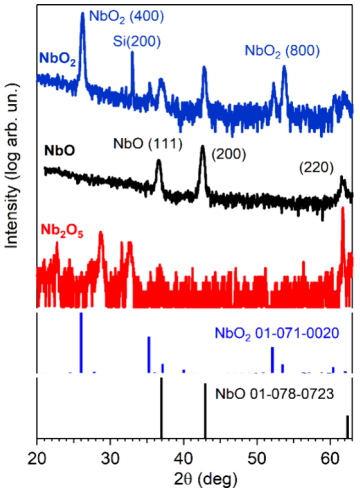

Figure 3. XRD 2θ-ω scans (in log scale) acquired on the niobium oxide film, after the thermal treatments detailed in Figure 1. The peaks from the JCPDS cards of the NbO and NbO_2 phases used as references for the assignment are also shown.

The NbO_2 XRD pattern (blue line in Figure 3) shows a very intense peak at 26°, related to NbO_2 (400), and the corresponding peak related to NbO_2(800) (JCPDS 01-071-0020). The prevalence of these peaks is related to a preferential [100] orientation. The other peaks at 35° and 52°, with a markedly lower intensity, can be related to other NbO_2 orientations. The peak at 42.5° is assigned to a minority NbO phase still present in the film, possibly originating from a noncomplete reoxidation. This phase is likely located in the deeper layers below the surface, since it is not visible in the XPS spectra of Figure 2c, consistent with the idea that reoxidation starts from the surface and a minority fraction of the film bulk is left in the NbO phase. The weak and narrow substrate-related peak appearing in the NbO_2 diffractogram derives from a forbidden Bragg-reflection. Its presence is critically dependent on sample alignment. The XRD spectra confirm the expected polycrystalline nature of the films. The coherence length has been determined from the full width at half-maximum of the Bragg peaks using the Scherrer formula,[40] which indicates that the average crystallite size is similar for the three films: approximately 15 nm for Nb_2O_5 and NbO, 24 nm for NbO_2.

The UV−vis absorptance spectra of the films are shown in Figure 4a. The Nb_2O_5 film (red line) shows an absorptance

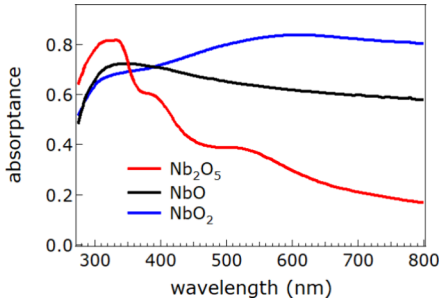

Figure 4. UV−visible absorptance spectra of the niobium oxide film after the thermal treatments detailed in Figure 1.

peak in the near UV with a maximum at 300−350 nm, related to transitions from the O 2p valence band to the Nb 4d conduction band. At higher wavelengths the absorptance decreases reaching values below 0.2 at 800 nm. The overall behavior is consistent with the trend observed in the literature for Nb_2O_5 reference compounds.[41] The spectrum shows some additional oscillations that are ascribed to interference effects, often observed in slightly absorbing thin films.[42] A reliable evaluation of the band gap is partially hindered by the presence of such oscillations.

The UV−vis spectra of the NbO (black line) and NbO_2 films (blue line) expectedly show a much higher absorptance in the visible range than the Nb_2O_5 film. In particular, the NbO film shows a maximum above 300 nm and a mild decrease of absorptance at higher wavelengths in the visible range. In the NbO_2 sample case the absorptance slightly increases in the

https://doi.org/10.1021/acs.jpcc.4c08535
J. Phys. Chem. C 2025, 129, 8206−8214

300−600 nm range and it decreases smoothly at higher wavelengths, in agreement with previous works on NbO_2 films.[43]

Figure 5 shows the SEM images of the surface morphology of the three films. The Nb_2O_5 film (Figure 5a) shows a

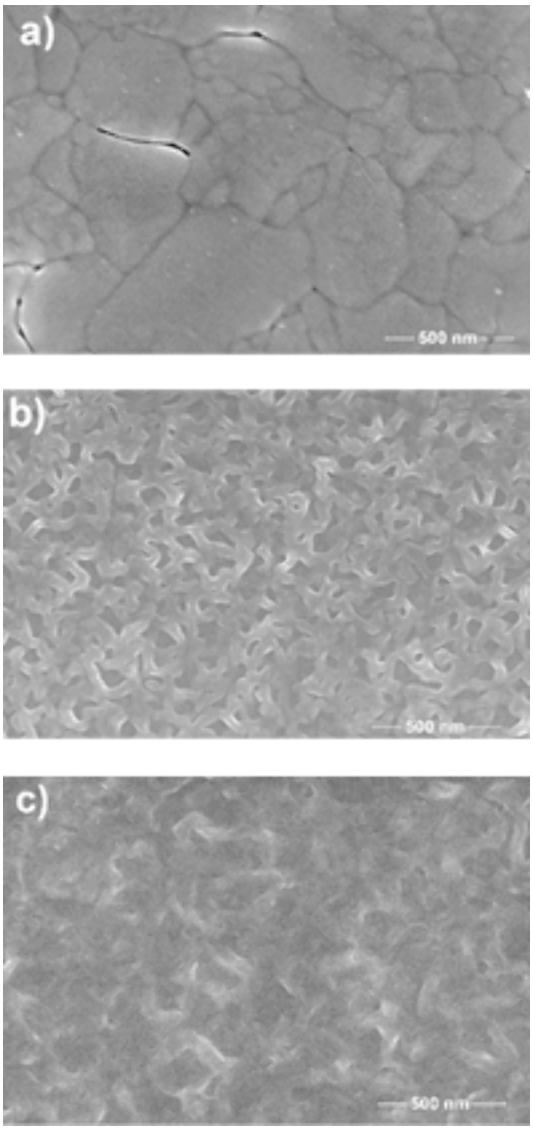

Figure 5. SEM images acquired on the niobium oxide film, after the thermal treatments detailed in Figure 1: (a) Nb_2O_5, (b) NbO, and (c) NbO_2.

nonuniform granular surface morphology with grains having a lateral size varying from tens of nm to several hundred nm and an irregular shape, induced by the thermal treatment at 600 °C in O_2 flow. The heat treatment at the same temperature in vacuum, that leads to NbO formation, instead brings a significantly different surface morphology (Figure 5b), with regular interconnected maze-like domains with a width of the order of 100 nm and dense irregular holes of comparable size. The NbO_2 film (Figure 5c) has a similar surface morphology as the NbO film, although the contrast of the SEM image is lower than in Figure 5b, showing that the oxidation in UHV-compatible conditions at slightly higher temperatures (750 °C) does not significantly alter the surface morphology.

Figure 6 shows the Nb K-edge XANES spectra of the film after oxidation in O_2/N_2 flux (Nb_2O_5) and after UHV

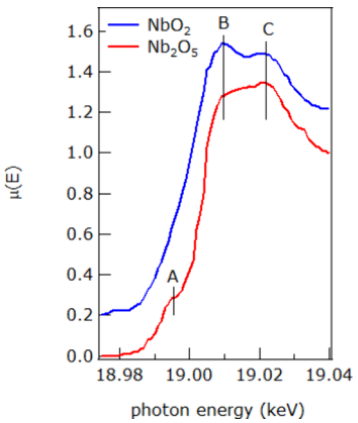

Figure 6. Nb K-edge XANES spectra of the Nb_2O_5 film after oxidation in O_2/N_2 flux (red curve) and of the NbO_2 film obtained after UHV reduction and reoxidation in UHV-compatible oxygen partial pressure (blue curve), as detailed in Figure 1.

reduction and reoxidation in UHV-compatible oxygen partial pressure (NbO_2). The investigations by FEL-based XANES were limited to the two semiconducting Nb_2O_5 and NbO_2 phases, on which future studies of photoexcited states may provide insight into challenging questions. In the Nb_2O_5 spectrum a broad pre-edge feature (A in Figure 6) is visible at 18.995 keV, ascribed to dipole−forbidden 1s → 4d transitions that become allowed due to local structural distortions that break the inversion symmetry and by the hybridization between the Nb 4d and 5p levels and the O 2p levels.[44] The two relatively broad and intense edge features (B and C in Figure 6) are related to 1s → 4p transitions, in which the absorption coefficient of Nb is modulated by scattering effects involving the second and the first coordination shell of the Nb atom, respectively.[45,46] The overall shape of the spectrum shown in Figure 6 is compatible with the spectrum measured on reference Nb_2O_5 powders (see Supporting Information, Figure S5) and with those reported in the literature for Nb_2O_5.[47,48] In the XANES spectrum of the film obtained by UHV reduction and reoxidation in UHV-compatible oxygen partial pressure conditions, the A pre-edge feature is not clearly observed, likely being too close to the main absorption edge and cannot be resolved from the B feature. Overall, the spectrum is compatible with those observed in the literature for NbO_2 films.[47,48] The edge positions were measured considering the maximum of the first derivative of the spectra. The NbO_2 film edge position (19,000 eV) is 3 eV below the Nb_2O_5 one (19,003 eV), with the shift being compatible with the one reported in the literature for reference compounds[49] and the Nb_2O_5 edge position being compatible with the one observed on reference Nb_2O_5 powders (Supporting Information, Figure S5). The comparison between XANES and XPS spectra allows to have information on the differences in composition of the film bulk and surface. XANES measurements at the Nb−K edge are in fact sensitive to the whole film thickness due to the large probing depth of high energy X-rays, while XPS with Al K_α photons is a very surface sensitive technique with a probing depth limited to a few nm. The XANES spectrum of the NbO_2 film, showing features related to Nb^{4+} ions, indicates that the

https://doi.org/10.1021/acs.jpcc.4c08535
J. Phys. Chem. C 2025, 129, 8206−8214

non-negligible concentration of Nb^{5+} ions observed by XPS in the NbO_2 film is confined on the film surface and it has a negligible weight when the whole film is probed.

The energy resolution of the XANES spectra shown in Figure 6 is limited by the short lifetime of the Nb K-edge core-hole. In spite of this limitation, the XANES spectra are sensitive to the electronic structure of Nb in the two different films. We underline that the spectra in Figure 6 have been acquired using ultrashort photon bunches in relatively short times, of the order of 10 min, achieving a signal-to-noise ratio of the order of 10^{-3} (see also Supporting Information, Figure S6). This evidence opens up the possibility of performing pump−probe XANES studies of the dynamic modifications of the electronic structure in such films with subps time resolution, in view for example of assessing the dynamics of photoexcitation in Nb_2O_5 or the light-induced phase IMT transition in NbO_2.

Considering possible future experiments by time-resolved XANES following photoexcitation, the IMT in the NbO_2 film was investigated by FTAS. The measurements were performed by collecting transient absorption (TA) spectra in the Vis-NIR and in different excitation regimes, changing fluence and wavelength of the pump pulse. Figure 7a reports TA spectra collected at selected time delays (0.1, 0.2, 0.3, 0.5, 1.0, and 2.0 ps) and acquired with a pump at 535 nm, with a fluence of 6.6 mJ/cm^2 (the complete false-color map is reported in Figure S6 of SI). The TA spectra show a large negative signal of photoinduced absorption (PIA) in the 400−1600 nm probe wavelength range. This PIA signal is due to absorption of photoexcited states in the NbO_2 film and it has temporal dynamics related to the excited carrier dynamics in these photoexcited states.

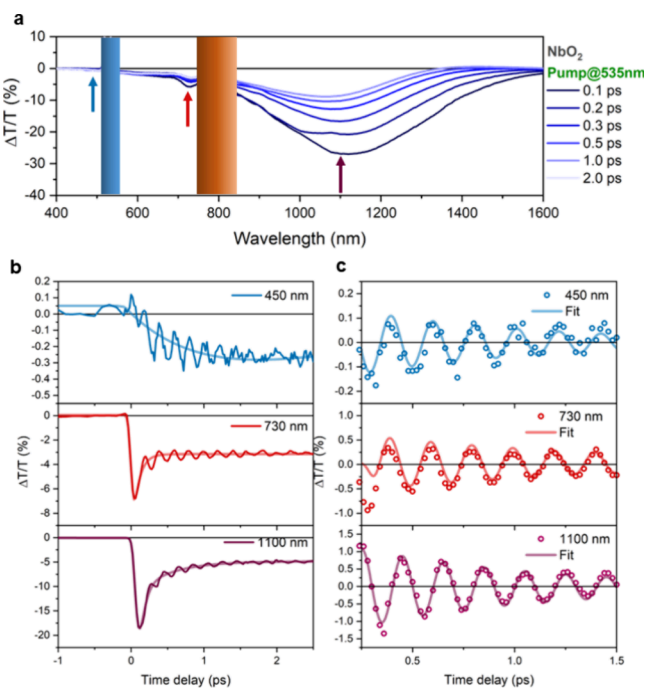

Figure 7. (a) TA spectra of the NbO_2 film at the pump photon wavelength of 535 nm and a pump fluence of 6.6 mJ/cm^2 at selected time delays (0.1, 0.2, 0.3, 0.5, 1.0, and 2.0 ps). The vertical blue band and orange bands cover the pump scattering and the spectral region without white light, respectively; (b) temporal dynamics of the transient signal obtained at the probe wavelength of 450 nm (blue), 730 nm (red), and 1100 nm (violet). Full lines represent experimental data while semitransparent lines represent the fitting of the incoherent dynamics; (c) oscillatory components of the TA signal due to the modulation by coherent phonons obtained at the probe wavelength of 450 nm (blue), 730 nm (red), and 1100 nm (violet). Scatter points represent experimental data while semitransparent lines represent the fitting of the oscillation due to excitation of coherent phonons.

Figure 7b shows the temporal dynamics obtained at selected probe energies that reveal oscillatory features in the transient signal. This oscillation was analyzed by subtracting the incoherent decay dynamics from the signal and isolating the oscillatory behavior due to the excitation of coherent phonons. These oscillations persist across a range of excitation fluences and are observed for pump wavelengths at 535 and 800 nm, while they disappear at both shorter (370 nm) and longer wavelengths (1150 nm). The invariance of the oscillation frequency across excitation fluences suggests that these oscillations are tied to the excitation of coherent optical phonons. Table 1 reports all the results obtained in the different excitation regimes.

Table 1. Frequency of the Excited Coherent Phonons Obtained for NbO_2 Samples Excited with Different Optical Pump Wavelengths and Fluences and Probed at Different Wavelengths

pump wavelength (nm)	probe wavelength (nm)	fluence (mJ/cm^2)	wavenumber (cm^{-1})
535	450	6.6	162 ± 2
535	730	6.6	166 ± 2
535	1100	6.6	167 ± 1
535	730	8.8	164 ± 1
535	730	22	161 ± 1
800	1100	22	163 ± 3

The average oscillatory wavenumber obtained in the different conditions is (165 ± 3) cm^{-1}, that likely indicates a lattice vibration mode strongly coupled to the electronic system, as observed also in the case of other systems.[50,51] An optical phonon mode in NbO_2 films is observed at a frequency of 165 cm^{-1} in literature studies.[17] The results shown in Figure 7 are compatible with those obtained by Wang et al.,[12] who attributed the coherent phonon modes in the NbO_2 film to Nb atomic motions within dimers, demonstrating that the films with dominant NbO_2 stoichiometry here investigated, reproduce the excited state behavior reported for state-of-the-art NbO_2 films.

The power dependence performed at 535 nm pump wavelength in the fluence range of 1−35 mJ/cm^2 is reported in Figure 8 together with the linear fit of the two different slopes shown by the data.

The data present a slope change at fluences around 12 mJ/cm^2. This change is attributed to an IMT by the literature.[11] At this fluence, Wang et al. observe that the transient signal at 6 μm begins to increase sharply near the threshold fluence indicating a sudden narrowing of the band gap.[12] Furthermore, the result is also consistent with the photoinduced nonthermal metallization of a NbO_2 film proposed in the fluence range from 10 to 17.5 mJ/cm^2.[11] An interesting point to note from Table 1 is that the frequencies of the emitted phonons do not significantly change on going from below to above the IMT threshold. These phonons are associated with Nb atomic motions within dimers which is precisely the motion that

https://doi.org/10.1021/acs.jpcc.4c08535
J. Phys. Chem. C 2025, 129, 8206−8214

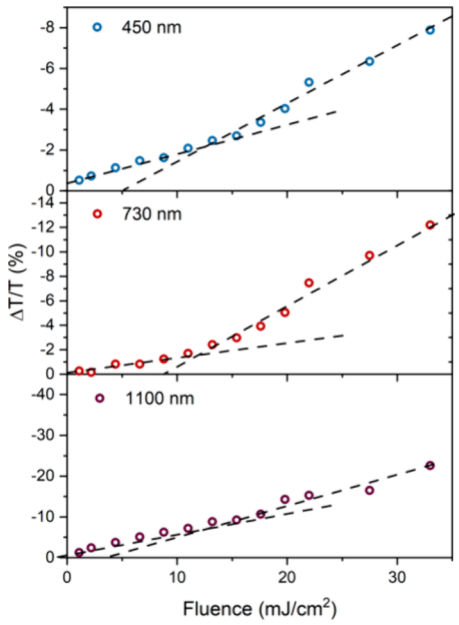

Figure 8. Transient intensity obtained at the time delay of 1.5 ps and probed at the pump photon wavelength of 535 nm and probe photon wavelength of 450 nm (blue scatter), 730 nm (red scatter), and 1100 nm (violet scatter) as a function of the pump fluence. Dashed lines represent the linear fits obtained at both low and high fluence regimes.

Kulmuss et al. suggest is involved in a Peierls-type transition in NbO_2.[10] In this picture our experimental results would be more consistent with a Mott-dominated behavior.[12] In addition, the spectral response of the film remains the same below and above the threshold, suggesting that the IMT does not permanently change the material and that the transition is reversible. These evidence make NbO_2 an intriguing candidate for further investigations, particularly using pump−probe XANES and X-ray or ultrafast electron diffraction techniques, to unravel the underlying dynamics of its phase transitions and to disentangle electronic and structural contributions definitively.

CONCLUSIONS

The present study demonstrated that using magnetron sputtering it is possible to obtain niobium oxide films and to modify their stoichiometry by heating treatments in vacuum, obtaining oxide films with Nb in one of its three most stable oxidation states. In particular, a thermal treatment at 600 °C in UHV reduces the film to the NbO stoichiometry, while a controlled heating treatment at 750 °C in O_2 in UHV-compatible conditions leads to the NbO_2 stoichiometry. The structure and stoichiometry of the Nb_2O_5 phase can be optimized by a heating treatment at 600 °C in O_2/N_2 flux. The femtosecond transient absorbance spectroscopy performed on the NbO_2 film shows evidence of the excitation of coherent phonons of 165 cm^{-1} and the optical pump power dependence studies presented are consistent with a photoinduced insulator to metal transition occurring in this material at 12 mJ/cm^2. The frequency of the emitted phonons does not significantly change on going from below to above this threshold suggesting that structural changes may not be heavily involved in the IMT, but this conclusion would need to be confirmed by other ultrafast techniques sensitive to the structure and electronic properties of the individual elements, such as time-resolved XANES studies. The films obtained represent good candidates on which to assess the light-induced ultrafast evolution of the properties. The feasibility of such studies is demonstrated by the Nb−K edge XANES measurements obtained using ultrashort XFEL pulses.

ASSOCIATED CONTENT

Supporting Information

The Supporting Information is available free of charge at https://pubs.acs.org/doi/10.1021/acs.jpcc.4c08535.

Nb 3d XPS fitting parameters; XPS spectra at different emission angles; comparison of Nb K-edge XANES in Nb_2O_5 powders and film; signal-to-noise ratio in Nb K-edge XANES of Nb_2O_5 film; and FTAS map (PDF)

AUTHOR INFORMATION

Corresponding Author

Paola Luches − *Istituto Nanoscienze, Consiglio Nazionale delle Ricerche, 41125 Modena, Italy;* orcid.org/0000-0003-1310-5357; Email: paola.luches@nano.cnr.it

Authors

Samuele Pelatti − *Dipartimento di Fisica Informatica e Matematica, Università di Modena e Reggio Emilia, 41121 Modena, Italy; Istituto Nanoscienze, Consiglio Nazionale delle Ricerche, 41125 Modena, Italy*

Stefania Benedetti − *Istituto Nanoscienze, Consiglio Nazionale delle Ricerche, 41125 Modena, Italy;* orcid.org/0000-0002-2683-4818

Giuseppe Ammirati − *Istituto di Struttura della Materia−CNR, EuroFEL Support Laboratory (EFSL), 00133 Rome, Italy*

Patrick O'Keeffe − *Istituto di Struttura della Materia−CNR, EuroFEL Support Laboratory (EFSL), 00133 Rome, Italy;* orcid.org/0000-0002-8676-4436

Daniele Catone − *Istituto di Struttura della Materia−CNR, EuroFEL Support Laboratory (EFSL), 00133 Rome, Italy;* orcid.org/0000-0002-7649-2756

Stefano Turchini − *Istituto di Struttura della Materia−CNR, EuroFEL Support Laboratory (EFSL), 00133 Rome, Italy*

Xinchao Huang − *European XFEL, 22869 Schenefeld, Germany*

Yohei Uemura − *European XFEL, 22869 Schenefeld, Germany;* orcid.org/0000-0003-3164-7168

Frederico Lima − *European XFEL, 22869 Schenefeld, Germany;* orcid.org/0000-0001-8106-2892

Christopher Jackson Milne − *European XFEL, 22869 Schenefeld, Germany;* orcid.org/0000-0003-4714-9139

Complete contact information is available at: https://pubs.acs.org/10.1021/acs.jpcc.4c08535

Notes

The authors declare no competing financial interest.

ACKNOWLEDGMENTS

Supported by the Italian Ministry of Foreign Affairs and International Cooperation (MAECI) under the program 2023 Italy − Germany Science and Technology Cooperation − project "Ultrafast Dynamics in Materials for Energy Conversion (U-DYNAMEC, CUP B53C23006060001)". S.T. and G.A. acknowledge funding from the European Union −

NextGenerationEU, M4C2, within the PNRR project NFFA-DI, CUP B53C22004310006, IR0000015.

REFERENCES

(1) Music, D.; Krause, A. M.; Olsson, P. A. T. Theoretical and Experimental Aspects of Current and Future Research on NbO2 Thin Film Devices. *Crystals* **2021**, *11* (2), 217.
(2) Lin, J.; Zhao, S.; Jervis, R.; Shearing, P. Probing the Electrochemical Processes of Niobium Pentoxides (Nb2O5) for High-Rate Lithium-ion Batteries: A Review. *ChemElectroChem* **2024**, *11* (6), No. e202300581.
(3) Nowak, I.; Ziolek, M. Niobium Compounds: Preparation, Characterization, and Application in Heterogeneous Catalysis. *Chem. Rev.* **1999**, *99* (12), 3603−3624.
(4) Li, T.; Nam, G.; Liu, K.; Wang, J.-H.; Zhao, B.; Ding, Y.; Soule, L.; Avdeev, M.; Luo, Z.; Zhang, W.; et al. A niobium oxide with a shear structure and planar defects for high-power lithium ion batteries. *Energy Environ. Sci.* **2022**, *15* (1), 254−264.
(5) Su, K.; Liu, H.; Gao, Z.; Fornasiero, P.; Wang, F. Nb2O5-Based Photocatalysts. *Adv. Sci.* **2021**, *8* (8), No. 2003156.
(6) Zhao, Y.; Zhou, X.; Ye, L.; Chi Edman Tsang, S. Nanostructured Nb2O5 catalysts. *Nano Rev.* **2012**, *3* (1), 17631.
(7) Hulm, J. K.; Jones, C. K.; Hein, R. A.; Gibson, J. W. Superconductivity in the TiO and NbO systems. *Journal of Low Temperature Physics* **1972**, *7* (3), 291−307.
(8) Nico, C.; Rino, L.; Matos, M.; Monteiro, R.; Costa, F. M.; Monteiro, T.; Graça, M. P. F. NbO/Nb2O5 core−shells by thermal oxidation. *Journal of the European Ceramic Society* **2013**, *33* (15), 3077−3083.
(9) Biermann, S.; Poteryaev, A.; Lichtenstein, A. I.; Georges, A. Dynamical Singlets and Correlation-Assisted Peierls Transition in VO_2. *Phys. Rev. Lett.* **2005**, *94* (2), No. 026404.
(10) Kulmus, K.; Gemming, S.; Schreiber, M.; Pashov, D.; Acharya, S. Theoretical evidence for the Peierls transition in NbO_2. *Phys. Rev. B* **2021**, *104* (3), No. 035128.
(11) Rana, R.; Klopf, J. M.; Grenzer, J.; Schneider, H.; Helm, M.; Pashkin, A. Nonthermal nature of photoinduced insulator-to-metal transition in NbO_2. *Phys. Rev. B* **2019**, *99* (4), No. 041102.
(12) Wang, Y.; Nie, Z.; Shi, Y.; Wang, Y.; Wang, F. Coherent vibrational dynamics of NbO_2 film. *Physical Review Materials* **2022**, *6* (3), No. 035005.
(13) Music, D.; Krause, A. M.; Olsson, P. A. T. Theoretical and Experimental Aspects of Current and Future Research on NbO2 Thin Film Devices. *Crystals* **2021**, *11*, 217.
(14) Weibin, Z.; Weidong, W.; Xueming, W.; Xinlu, C.; Dawei, Y.; Changle, S.; Liping, P.; Yuying, W.; Li, B. The investigation of NbO2 and Nb2O5 electronic structure by XPS, UPS and first principles methods. *Surf. Interface Anal.* **2013**, *45* (8), 1206−1210.
(15) Ücker, C. L.; Gularte, L. T.; Fernandes, C. D.; Goetzke, V.; Moreira, E. C.; Raubach, C. W.; Moreira, M. L.; Cava, S. S. Investigation of the properties of niobium pentoxide for use in dye-sensitized solar cells. *J. Am. Ceram. Soc.* **2019**, *102* (4), 1884−1892.
(16) Ai, W.; Xiong, S. Structural and optical properties of Nb2O5 films prepared by dual ion assisted deposition. *Optics & Laser Technology* **2022**, *150*, No. 107850.
(17) Hossain, N.; Günes, O.; Zhang, C.; Koughia, C.; Li, Y.; Wen, S.-J.; Wong, R.; Kasap, S.; Yang, Q. Structural and physical properties of NbO2 and Nb2O5 thin films prepared by magnetron sputtering. *Journal of Materials Science: Materials in Electronics* **2019**, *30* (10), 9822−9835.
(18) Posadas, A. B.; O'Hara, A.; Rangan, S.; Bartynski, R. A.; Demkov, A. A. Band gap of epitaxial in-plane-dimerized single-phase NbO2 films. *Appl. Phys. Lett.* **2014**, *104* (9), No. 092901.
(19) Deng, X.; Zhang, J.; Qi, K.; Liang, G.; Xu, F.; Yu, J. Ultrafast electron transfer at the In2O3/Nb2O5 S-scheme interface for CO2 photoreduction. *Nat. Commun.* **2024**, *15* (1), 4807.
(20) Ren, X.; Shi, J.; Duan, R.; Di, J.; Xue, C.; Luo, X.; Liu, Q.; Xia, M.; Lin, B.; Tang, W. Construction of high-efficiency CoS@Nb2O5 heterojunctions accelerating charge transfer for boosting photocatalytic hydrogen evolution. *Chin. Chem. Lett.* **2022**, *33* (10), 4700−4704.
(21) Wegkamp, D.; Herzog, M.; Xian, L.; Gatti, M.; Cudazzo, P.; McGahan, C. L.; Marvel, R. E.; Haglund, R. F.; Rubio, A.; Wolf, M.; et al. Instantaneous Band Gap Collapse in Photoexcited Monoclinic VO_2 due to Photocarrier Doping. *Phys. Rev. Lett.* **2014**, *113* (21), No. 216401.
(22) Morrison, V. R.; Chatelain, R. P.; Tiwari, K. L.; Hendaoui, A.; Bruhács, A.; Chaker, M.; Siwick, B. J. A photoinduced metal-like phase of monoclinic VO_2 revealed by ultrafast electron diffraction. *Science* **2014**, *346* (6208), 445.
(23) Beebe, M. R.; Klopf, J. M.; Wang, Y.; Kittiwatanakul, S.; Lu, J.; Wolf, S. A.; Lukaszew, R. A. Time-resolved light-induced insulator-metal transition in niobium dioxide and vanadium dioxide thin films. *Opt. Mater. Express* **2017**, *7* (1), 213−223.
(24) O'Hara, A.; Demkov, A. A. Nature of the metal-insulator transition in NbO_2. *Phys. Rev. B* **2015**, *91* (9), No. 094305.
(25) Clark, J. K.; Ho, Y.-L.; Matsui, H.; Tabata, H.; Delaunay, J.-J. Thresholdless behavior and linearity of the optically induced metallization of NbO_2. *Physical Review Research* **2019**, *1* (3), No. 033168.
(26) Joshi, T.; Senty, T. R.; Borisov, P.; Bristow, A. D.; Lederman, D. Preparation, characterization, and electrical properties of epitaxial NbO2 thin film lateral devices. *J. Phys. D: Appl. Phys.* **2015**, *48* (33), No. 335308.
(27) Gallego, J. M.; Thomas, C. B. Preparation and characterization of thin films of NbO2. *Thin Solid Films* **1982**, *98* (1), 11−22.
(28) Yoshimura, K.; Miki, T.; Iwama, S.; Sakae Tanemura, S. T. Niobium Oxide Electrochromic Thin Films Prepared by Reactive DC Magnetron Sputtering. *Jpn. J. Appl. Phys.* **1995**, *34* (10A), L1293.
(29) Wong, F. J.; Hong, N.; Ramanathan, S. Orbital splitting and optical conductivity of the insulating state of NbO_2. *Phys. Rev. B* **2014**, *90* (11), No. 115135.
(30) Yoshimura, K.; Miki, T.; Iwama, S.; Tanemura, S. Characterization of niobium oxide electrochromic thin films prepared by reactive d.c. magnetron sputtering. *Thin Solid Films* **1996**, *281−282*, 235−238.
(31) Venkataraj, S.; Drese, R.; Kappertz, O.; Jayavel, R.; Wuttig, M. Characterization of Niobium Oxide Films Prepared by Reactive DC Magnetron Sputtering. *physica status solidi (a)* **2001**, *188* (3), 1047−1058.
(32) Graça, M. P. F.; Saraiva, M.; Freire, F. N. A.; Valente, M. A.; Costa, L. C. Electrical analysis of niobium oxide thin films. *Thin Solid Films* **2015**, *585*, 95−99.
(33) Logacheva, V. A.; Divakova, N. A.; Tikhonova, Y. A.; Dolgopolova, E. A.; Khoviv, A. M. Growth of niobium oxide films on single-crystal silicon. *Inorg. Mater.* **2007**, *43* (11), 1230−1234.
(34) King, B. R.; Patel, H. C.; Gulino, D. A.; Tatarchuk, B. J. Kinetic measurements of oxygen dissolution into niobium substrates: In situ X-ray photoelectron spectroscopy studies. *Thin Solid Films* **1990**, *192* (2), 351−369.
(35) Fontaine, R.; Caillat, R.; Feve, L.; Guittet, M. J. Déplacement chimique ESCA dans la série des oxydes du niobium. *J. Electron Spectrosc. Relat. Phenom.* **1977**, *10* (4), 349−357.
(36) Magnozzi, M.; Proietti Zaccaria, R.; Catone, D.; O'Keeffe, P.; Paladini, A.; Toschi, F.; Alabastri, A.; Canepa, M.; Bisio, F. Interband Transitions Are More Efficient Than Plasmonic Excitation in the Ultrafast Melting of Electromagnetically Coupled Au Nanoparticles. *J. Phys. Chem. C* **2019**, *123* (27), 16943−16950.
(37) Khakhulin, D.; Otte, F.; Biednov, M.; Bömer, C.; Choi, T.-K.; Diez, M.; Galler, A.; Jiang, Y.; Kubicek, K.; Lima, F. A.; et al. Ultrafast X-ray Photochemistry at European XFEL: Capabilities of the Femtosecond X-ray Experiments (FXE) Instrument. *Appl. Sci.* **2020**, *10*, 995.
(38) Galler, A.; Gawelda, W.; Biednov, M.; Bomer, C.; Britz, A.; Brockhauser, S.; Choi, T.-K.; Diez, M.; Frankenberger, P.; French, M.; et al. Scientific instrument Femtosecond X-ray Experiments (FXE): instrumentation and baseline experimental capabilitiesThis article will

https://doi.org/10.1021/acs.jpcc.4c08535
J. Phys. Chem. C 2025, 129, 8206−8214

form part of a virtual special issue on X-ray free-electron lasers. *Journal of Synchrotron Radiation* **2019**, *26* (5), 1432−1447.
(39) Grundner, M.; Halbritter, J. XPS and AES studies on oxide growth and oxide coatings on niobium. *J. Appl. Phys.* **1980**, *51* (1), 397−405.
(40) Scherrer, P. Bestimmung der Größe und der inneren Struktur von Kolloidteilchen mittels Röntgenstrahlen. *Nachrichten von der Gesellschaft der Wissenschaften zu Göttingen, Mathematisch-Physikalische Klasse* **1918**, *2*, 98−100.
(41) Ambreen, S.; Pandey, N. D.; Chouhan, A.; Kumar, H.; Pandey, A. Effect of chelation in alkoxide precursors of niobium oxide nanoparticles on photochemical degradation of rhodamine B. *J. Sol-Gel Sci. Technol.* **2021**, *98* (2), 319−334.
(42) Amotchkina, T. V.; Trubetskov, M. K.; Tikhonravov, A. V.; Janicki, V.; Sancho-Parramon, J.; Razskazovskaya, O.; Pervak, V. Oscillations in spectral behavior of total losses (1−R−T) in thin dielectric films. *Opt. Express* **2012**, *20* (14), 16129−16144.
(43) Nakao, S.; Kamisaka, H.; Hirose, Y.; Hasegawa, T. Structural, electrical, and optical properties of polycrystalline NbO2 thin films grown on glass substrates by solid phase crystallization. *Phys. Status Solidi A* **2017**, *214* (3), No. 1600604.
(44) Getty, K.; Delgado-Jaime, M. U.; Kennepohl, P. Assignment of pre-edge features in the Ru K-edge X-ray absorption spectra of organometallic ruthenium complexes. *Inorg. Chim. Acta* **2008**, *361* (4), 1059−1065.
(45) Bollaert, Q.; Chassé, M.; Morin, G.; Baptiste, B.; Courtin, A.; Galoisy, L.; Landrot, G.; Quantin, C.; Calas, G. Atomic-scale environment of niobium in ore minerals as revealed by XANES and EXAFS at the Nb K-edge. *Eur. J. Mineral.* **2024**, *36* (1), 55−72.
(46) Piilonen, P. C.; Farges, F.; Linnen, R. L.; Brown, G. E. Tin and niobium in dry and fluid-rich (H2O, F) silicate glasses. *Phys. Scr.* **2005**, *2005* (T115), 405.
(47) Páez Fajardo, G. J.; Howard, S. A.; Evlyukhin, E.; Wahila, M. J.; Mondal, W. R.; Zuba, M.; Boschker, J. E.; Paik, H.; Schlom, D. G.; Sadowski, J. T.; et al. Structural Phase Transitions of NbO2: Bulk versus Surface. *Chem. Mater.* **2021**, *33* (4), 1416−1425.
(48) Ichikuni, N.; Yanagase, F.; Mitsuhara, K.; Hara, T.; Shimazu, S. Nb K- and L3-edges XAFS study on the structure of supported Nb carbide catalyst. *Journal of Physics: Conference Series* **2016**, *712* (1), No. 012060.
(49) Froideval, A.; Degueldre, C.; Segre, C. U.; Pouchon, M. A.; Grolimund, D. Niobium speciation at the metal/oxide interface of corroded niobium-doped Zircaloys: A X-ray absorption near-edge structure study. *Corros. Sci.* **2008**, *50* (5), 1313−1320.
(50) Lou, S.-T.; Zimmermann, F. M.; Bartynski, R. A.; Hur, N.; Cheong, S.-W. Femtosecond laser excitation of coherent optical phonons in ferroelectric $LuMnO_3$. *Phys. Rev. B* **2009**, *79* (21), No. 214301.
(51) Hasegawa, T.; Fujimura, N.; Nakayama, M. Ultrafast dynamics of coherent optical phonon correlated with the antiferromagnetic transition in a hexagonal YMnO3 epitaxial film. *Appl. Phys. Lett.* **2017**, *111* (19), 192901.

https://doi.org/10.1021/acs.jpcc.4c08535
J. Phys. Chem. C 2025, 129, 8206−8214